

## ITER Confinement and Stability Modelling

POLEVOI Alexei R., MEDVEDEV Sergei Yu.<sup>1</sup>, MUKHOVATOV Vladimir S., KUKUSHKIN Andrei S.<sup>2</sup>,  
MURAKAMI Yoshiki<sup>3</sup>, SHIMADA Michiya and IVANOV Andrei A.<sup>1</sup>

*ITER CTA, Naka JWS, Naka, 311-0193, Japan*

<sup>1</sup>*Keldysh Institute of Applied Mathematics, 125047 Moscow, Russian Federation*

<sup>2</sup>*ITER CTA, Garching JWS, Garching bei Munchen, Germany*

<sup>3</sup>*Power and Industrial Systems R&D Center, Toshiba Corp., Kawasaki 210-0862, Japan*

(Received: 11 December 2001 / Accepted: 18 April 2002)

### Abstract

The results of self-consistent transport and stability studies of the ITER reference inductive and steady-state reversed shear scenarios are discussed. The semi-empirical transport models used for ITER simulations with 1.5D transport codes ASTRA and PRETOR are described. The analysis reveals a weak dependence of plasma performance on the radial profiles of transport coefficients provided the coefficients are adjusted to make the computed energy confinement time equal to that given by a global H-mode scaling relation ( $H_H = 1$ ). It is shown that the ITER reference inductive scenario with  $Q = 10$ ,  $P_{\text{fus}} = 400$  MW,  $I_p = 15$  MA is stable against the high and low  $n$  ideal MHD modes without a conducting wall. Steady-state operation with  $Q > 5$  would require a reduced current  $I_p \sim 9$  MA, enhanced confinement with  $H_H \sim 1.5$ ,  $\beta_N \sim 3$ , high bootstrap fraction  $\sim 50\%$  and a reversed magnetic shear configuration. This configuration is ideally unstable without a wall and stable with a conducting wall at 1.4a.

### Keywords:

tokamak, transport, stability, ITER

### 1. Introduction

Predictions of plasma performance in ITER during the Engineering Design Activity (EDA) have been based largely on the empirical global confinement scalings while two other possible approaches, i.e. the dimensionless physics parameter scaling technique and application of physics-based transport models, have been used for comparison [1]. All these techniques have progressed well during recent years. In particular, the models based on transport governed by drift wave turbulence have demonstrated their capability to describe energy transport in the plasma core of L- and H-modes and predict the formation of internal transport barriers in some experiments [2-4]. These models show

a strong dependence of core plasma parameters on boundary conditions presently taken from experiments. The absence of a reliable model for the edge pedestal parameters reduces significantly the projection capability of these transport models.

In 1999, the ITER Confinement Database and Modelling Expert Group has recommended for ITER design the ITERH-98P(y,2) confinement scaling [5]

$$\tau_E^{\text{H98}(y,2)} = 0.0562 I^{0.93} B^{0.15} \bar{n}_{10}^{0.41} P^{-0.69} R^{1.97} \kappa_a^{0.78} \epsilon^{0.58} M^{0.19}, \quad (1)$$

where the units are s, MA, T,  $10^{19} \text{ m}^{-3}$ , MW, m, AMU. From recent analysis of the enlarged global confinement

Corresponding author's e-mail: polevoa@itergps.naka.jaeri.go.jp

database (ITERH.DB3), the practical reliability of the ITERH-98(y,2) scaling was confirmed, and the  $2\sigma$  log-linear interval was reduced from  $\pm 18$  to  $\pm 14\%$  [6]. The practical application of the global confinement scalings for ITER performance projection consists in normalising the plasma thermal diffusivities,  $\chi_i$  and  $\chi_e$ , used in 1.5D transport codes in such a way that the energy confinement time computed by the code coincides with that given by the scaling relation. The radial profiles of transport coefficients are chosen in a form that allows satisfactory description by the code of the temperature and density profiles in present experiments. An example of the results of such 1.5D simulations is shown in Fig. 1 where the ITER operation domain with  $Q = 10$  is represented on the plane  $P_{\text{fus}} - H_{\text{H98}(y,2)}$  [7]. Here  $Q \equiv P_{\text{fus}}/P_{\text{ADD}}$ ,  $P_{\text{fus}}$  is the fusion power,  $P_{\text{ADD}}$  is the auxiliary heating power,  $H_{\text{H98}(y,2)} = \tau_E/\tau_{E,H98(y,2)}$  is the confinement improvement factor relative to the scaling (1). Two models of this type used for ITER predictions are discussed in Sec. 1. The results of model benchmarking versus the discharges from the ITER profile database are presented.

Such a 1D treatment of the core transport requires some sort of boundary conditions at the core edge (separatrix). Modelling of the scrape-off layer (SOL) and divertor (DIV) requires at least a 2D consideration with neutral particle simulations by sophisticated Monte Carlo technique [8]. So, core boundary conditions have to be consistent with the SOL/DIV transport simulations and limitations. The operational window for boundary conditions and edge transport are discussed in Sec. 2. The sensitivity of model predictions to boundary

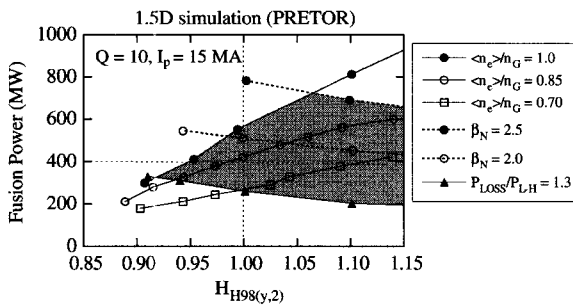


Fig. 1 Operational domain in  $H_{\text{H98}(y,2)}$ -factor/fusion power space for  $I_p = 15$  MA and  $Q = 10$ . Operational boundaries (shaded area) are given by  $\langle n_e \rangle / n_G = 1.0$ ,  $\beta_N = 2.5$  and  $P_{\text{LOSS}}/P_{\text{L-H}} = 1.3$  where  $n_G$  is the Greenwald density,  $n_G = I_p/(\pi a^2)$ ,  $P_{\text{LOSS}}$  is the power conducted and convected through the separatrix, and  $P_{\text{L-H}}$  is the H-mode power threshold.

conditions is discussed.

The core transport in the central zone with low safety factor  $q < 1$  is affected by sawtooth (ST) oscillations. In Sec. 2 we compare semi-empirical and theory-based ST model predictions for ITER. If the ST period is longer than the central zone temperature and density recovery time (as expected in ITER), then in a zone with low magnetic shear caused by ST mixing and high-pressure gradient, the ballooning mode stability limit may restrict plasma performance. The results of ballooning stability analysis for the reference inductive scenario are presented in Sec. 3.

To provide steady-state operation, low plasma current  $I \sim 9$  MA operation with high normalised-beta  $\beta_N \sim 3$  is required. In these regimes ideal MHD modes can be excited. The possibility of mode stabilisation by conducting wall for the SS scenario is discussed in Sec. 3.

So, the present analysis comprises semi-empirical model benchmarking versus the experimental profile database. We also consider the sensitivity of ITER plasma performance predictions to model assumptions such as the profile of diffusivity, boundary conditions, saw-tooth oscillations, He transport, and limitations caused by ballooning and ideal kink mode stability.

## 2. Core Transport Modelling

ITER performance simulations were carried out by PRETOR [9] and ASTRA [10] transport codes. Radial 1D transport of charged and neutral particles, electron and ion heat, toroidal momentum  $M_\phi$  and poloidal magnetic flux  $\psi$  was simulated with a self-consistent 2D equilibrium calculation. Such an approach is called 1.5D modelling.

In the reduced version, charged particle transport is simulated only for the electron and helium components  $n_e$  and  $n_{\text{He}}$ . Other impurity species are supposed to be known fractions of the electron density  $n_{zk} = f_k n_e$ , the fuel densities  $n_D$ ,  $n_T$  are calculated from the quasineutrality conditions:  $n_e = n_D + n_T + 2 n_{\text{He}} + \sum_k Z_k n_{zk}$ .

The electron source  $S_e$  is calculated from edge gas puffing, pellet and neutral beam NB injection modelling. The helium source  $S_{\text{He}}$  is defined from fusion reaction calculations and ionisation of the He atomic influx at the boundary. The impurity charge  $Z_k$  is determined from the coronal equilibrium model [11].

The poloidal magnetic flux  $\psi$  diffusion equation takes account of the bootstrap current density  $j_{\text{bs}}$  [12] and the externally driven current density  $j_{\text{CD}}$ .

### Transport coefficients

For the simulations of ITER performance, thermal, toroidal momentum and particle diffusivities,  $\chi_e$ ,  $\chi_i$ ,  $\chi_\phi$ ,  $D_{He}$ ,  $D_e$  of similar form are chosen:

$$D = C f(\rho) h(\rho) + (1 - h(\rho)) \chi^{neo}, \quad (2)$$

where  $h(\rho) = 1$  for  $\rho < 0.9$  and  $h(\rho) = 0$  for  $\rho > 0.9$  (corresponding to the H-mode edge pedestal transport improvement to neoclassical value),  $\rho = r/r_a$  is the normalised radius, connected with the toroidal magnetic flux  $\Phi$  ( $r = (\Phi/\pi B)^{1/2}$  and  $B$  is the toroidal magnetic field). For ITER scenarios this simplified description of the edge pedestal gives a pedestal pressure gradient within the ballooning limit which is consistent with the ELM-Type-I operation considered.

The relation between normalisation constants is chosen on the basis of experiments:  $\chi_i/\chi_e = 2$ ,  $\chi_i/\chi_\phi = 1$ ,  $D_e/\chi_e = 1$ ,  $D_{He}/D_e = 1$ . The normalisation is fitted to provide the prescribed behaviour of the energy confinement time  $\tau_E$  according to experimental scaling, i.e.  $H_{H98(y,2)} = 1$ .

In ASTRA simulations it was chosen in the simplest form approximating a radial dependence of the transport coefficients observed in experiments:

$$f(\rho) = 1 + 3 \rho^2. \quad (3)$$

In PRETOR simulations, the radial shape was chosen according to the transport model described in [13].

### Model validation

The semi-empirical ITER model with diffusivity profile (3) was benchmarked with the experimental data from the international profile data base [14]. The subset of experimental data with  $H_{H98} \sim 1$ , high density,  $n/n_G > 0.5$ , and flat density profiles was chosen for such benchmarking. The boundary conditions and input power profiles are taken from experiments. Heat and particle transport is simulated. The simulations reveal satisfactory agreement between ITER semi-empirical model predictions and experimentally-measured temperature profiles. For the considered data subset the average standard deviation ( $\Delta T_{std} = (\sum (T_s - T_x)^2) / (\sum T_x^2)^{1/2}$ ) is 14% for ions and 12% for electrons, where  $T_s$  is simulation,  $T_x$  is an experiment (summation is performed over the radial point positions).

### Boundary conditions

In PRETOR simulations relatively high density  $n_e \sim$

$6 \times 10^{19} \text{ m}^{-3}$  and temperature  $T \sim 1 \text{ keV}$  are used as boundary conditions for the reference inductive scenario simulations (see Fig. 2). In ASTRA the boundary conditions at the separatrix are calculated from interpolation of the B2-Eirene (B2E) calculations for SOL/DIV heat, charged and neutral particle transport. In this approach, the densities, temperatures of charged particles, as well as neutral fuel and impurities inflows are calculated self-consistently as functions of power output, and the outflows of DT, He and impurity ions:  $\Gamma_{DT,s}$ ,  $\Gamma_{He,s}$ ,  $\Gamma_{imp,s}$ . Proper control of plasma parameters is provided by realistic actuators: such as gas puffing rate  $\Gamma_0$ , pumping speed  $S_p$ , deep fuelling rate  $\Gamma_{core}$  (neutral beams (NB) [15], pellet injection), tritium fraction in the fuel and auxiliary heating power  $P_{ADD}$ . For the reference  $P_{fus} = 400 \text{ MW}$  inductive operation with loss power  $P_{LOSS} < 100 \text{ MW}$  this interpolation predicts rather low

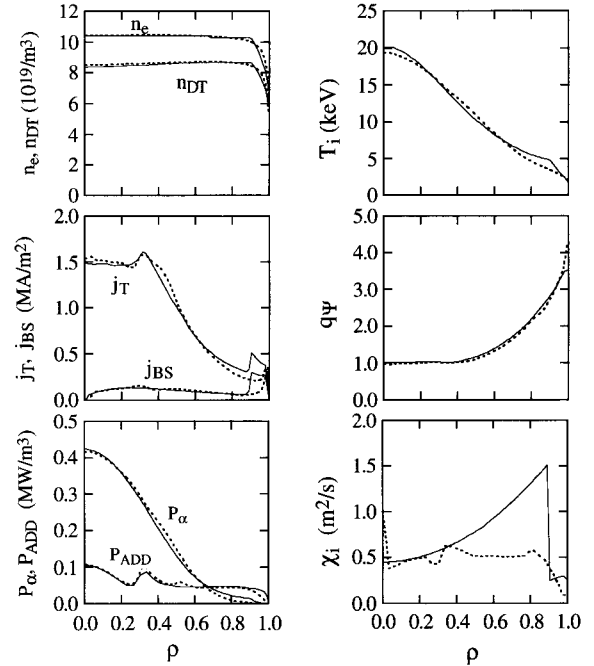


Fig. 2 Radial distribution of plasma parameters predicted for the same boundary conditions and  $\tau_{He}^*/\tau_E = 5$  by ASTRA (solid line) with the heat conductivity  $\chi$  profile described by Eqs. (2), (3), and by PRETOR (dashed line) with another  $\chi$  profile, described in Ref. [13].  $n_e$  and  $n_{DT}$  are electron and fuel ion densities,  $T_i$  is the ion temperature,  $j_T$ ,  $j_{BS}$  are the total and bootstrap current densities,  $q_\psi$  is the safety factor,  $P_{ADD}$ ,  $P_\alpha$  are the additional and alpha heating power densities. Corresponding global parameters are represented in the middle column of Table 1.

boundary density  $n_e(a) \sim 3 \times 10^{19} \text{ m}^{-3}$ , temperature  $T(a) \sim 200 \text{ eV}$  and He atomic influx  $\Gamma_{\text{He},0} \sim 0.5\text{--}0.6 \Gamma_{\text{He},s}$ .

Two different approaches were used for helium transport analysis. The simplest one supposes that recirculating atomic helium is completely ionised before reaching the core (i.e. the helium ions in the core originate from fusion only  $S_{\text{He}} = S_{\text{He},\text{fus}}$ ). The helium ion density is controlled independently by He pumping at the edge. In this approach the details of transport are not too important for the integral He contamination, since the He content is supposed to be controlled by pumping [16] to provide helium contamination at the desirable level  $\tau_{\text{He}}^*/\tau_E = 5$ , where  $\tau_{\text{He}}^* = \int n_{\text{He}} dV / \int S_{\text{He}} dV$ . The second approach is based on the B2-Eirene calculations. In this approach, the recirculating He atomic influx and the He boundary density are calculated self-consistently with particle and energy circulation in the SOL/DIV area. In that case the ratio  $\tau_{\text{He}}^*/\tau_E$  is the result of calculations rather than an input parameter.

#### Sawtooth oscillations

We consider two approaches for ST oscillations in ITER simulations. The semi-empirical, simplified model is used in ASTRA, where the ST mixing is supposed to be triggered by some specific current profile in the zone  $\rho_{\text{ST}} < 1.4 \rho$  ( $q = 1$ ). In PRETOR simulations the complete reconnection model by F. Porcelli *et al.* [17] is used for ST description. The ST is triggered when the perturbed magnetic energy exceeds some threshold  $\delta W_{\text{mag}} > W_{\text{thr}}$ , and the mixing radius  $\rho_{\text{ST}}$  is calculated from flux continuity. In both approaches particles and temperatures are flattened over the ST zone taking account of particle and energy conservation.

#### Sensitivity studies

Simulations reveal a weak sensitivity of plasma performance to the detailed shape of transport coefficients  $f(\rho)$  (see Fig. 2). For the same boundary conditions, the normalisation  $H_{\text{H98}} = 1$  gives transport which is similar in the hot central zone resulting in almost identical plasma parameter profiles.

The details of the ST modelling have a minor effect on plasma performance too, since the temperature and density profile recovery proceeds faster than plasma current profile recovery  $\tau_{\text{ST}} \gg \tau_E$  (ST period  $\sim$  mixing zone skin time). The performance dependence on the boundary conditions is much stronger (Fig. 3 and Table. 1).

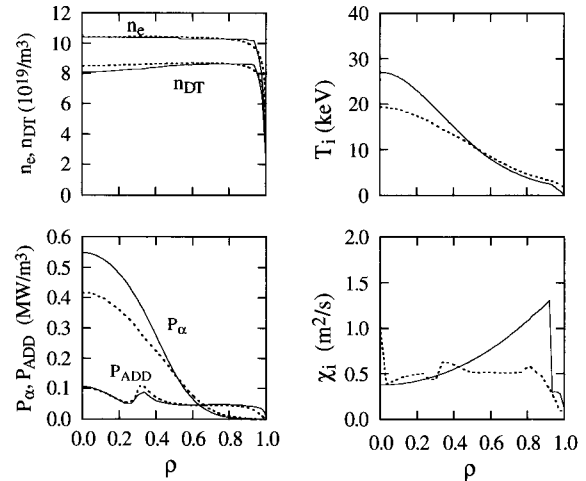


Fig. 3 Radial distribution of plasma parameters predicted by ASTRA (solid line) and PRETOR (dashed line) calculations for different boundary conditions and He transport.  $\chi$  is the heat conductivity,  $n_e$  and  $n_{\text{DT}}$  are the electron and fuel densities,  $T_i$  is the ion temperature,  $P_{\text{ADD}}$ ,  $P_\alpha$  are the additional and alpha heating power densities. The ASTRA modelling includes boundary conditions and He transport compatible with B2-Eirene calculations. Corresponding global parameters are represented in the last column of Table 1.

Table 1 Sensitivity of plasma performance to boundary conditions

	PRETOR&ASTRA	ASTRA+B2E
R/a (m/m)	6.2 / 2.0	6.2 / 2.0
$B_T$ (T)	5.3	5.3
$I_p$ (MA)	15.0	15.0
$\kappa_\chi / \delta_\chi$	1.7 / 0.33	1.7 / 0.33
$\langle n_e \rangle$ ( $10^{19} \text{ m}^{-3}$ )	10.1	10.1
$n/n_G$	0.85	0.84
$\langle T_i \rangle$ (keV)	8.0	8.9
$\langle T_e \rangle$ (keV)	8.8	9.7
$\beta_T$ (%)	2.49	2.78
$\beta_N$	1.76	1.97
$P_{\text{fus}}$ (MW)	400	471
$Q = P_{\text{fus}} / (P_{\text{NB}} + P_{\text{RF}})$	10	11.8
$W_{\text{th}}$ (MJ)	320	348
$P_{\text{LOSS}} / P_{\text{L-H}}$	1.8	1.9
$\tau_E$ (s)	3.71	3.45
$f_{\text{He,ave}}$ (%)	3.2	4.7
$Z_{\text{eff,ave}}$	1.66	1.69
$P_{\text{RAD}}$ (MW)	47	46
$l_i$	0.85	0.81
$\tau_{\text{He}}^* / \tau_E$	5.0	6.7

### 3. Ideal Mode Stability Analysis

The ballooning and low-n ideal kink mode stability was carried out using the KINX code [18]. The result of analysis of the ballooning stability between the ST oscillations in the reference inductive ITER scenarios is presented in Fig. 4. The analysis reveals that in the wide central ST mixing zone, the pressure gradient is close to the ballooning/Mercier stability limit  $p' \sim p'_{lim}$ . Possible excitation of ballooning modes in this case may affect plasma performance and would require further analysis.

Steady state (SS) operation with high  $Q > 5$  and moderate internal inductance  $l_i \sim 0.6-0.7$  requires high beta  $\beta_N > 4 l_i$  operation, where the ideal kink modes become unstable without a conducting wall. A high bootstrap current fraction in SS operation produces reversed shear configurations  $q(0) > q_{min}$  (Fig. 5). SS is possible for the same global parameters: geometry,  $B$ ,  $I_p$ ,  $n_e$  with different safety factor profiles (different  $q_{min}$ ) and multiplication factor  $Q$  (which decreases when  $q_{min}$  increases) controlled by a variation of lower hybrid current drive. The maximum distance to the conducting wall that can provide the kink mode stabilisation

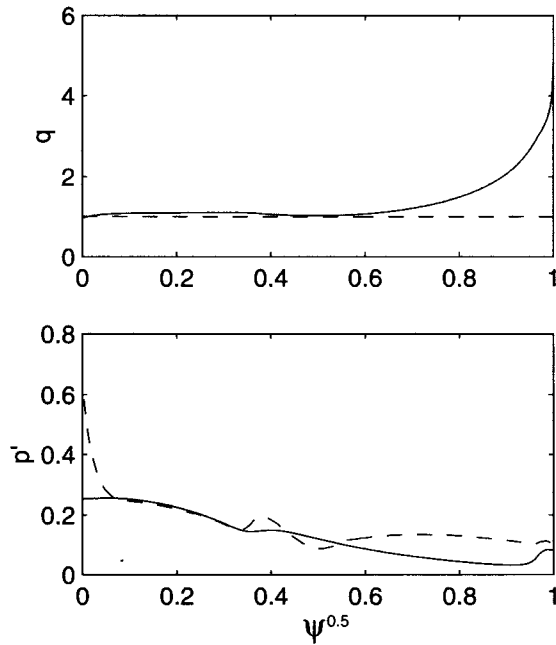


Fig. 4 Safety factor  $q$  (top) and pressure gradient  $p'$  (bottom) radial profiles before sawtooth mixing. Pressure gradient given by transport simulation is shown by solid line and the ballooning/Mercier stability limit is shown by a dashed line. The normalised square root of the poloidal flux is used as the radial variable.

increases with  $q_{min}$ . So, the ITER wall position,  $a_w/a \approx 1.4$  for  $a = 1.85$  m, implies a lower limit on  $q_{min}$  (upper limit on  $Q$ ) for chosen global parameters.

The results of stability analysis for equilibria with scaled pressure profile (and  $\beta_N$ ) with fixed  $q$  profile for different  $q_{min}$  for the SS operational regimes presented in Table 2 are shown in Fig. 6. The operational parameters in Table 2 are calculated for  $R = 6.35$  m,  $a = 1.85$  m,  $\delta_{95}/k_{95} = 0.41/1.84$ ,  $B = 5.175$  T,  $I_p = 9$  MA,  $\langle n_e \rangle = 6.74 \times 10^{19} \text{m}^{-3}$ ,  $P_{NB} = 34$  MW with the neoclassical ion heat diffusivity in the reversed shear zone.

The calculations reveal that the operational point with  $\beta_N = 2.8$  for  $q_{min} = 2.1$  is located in the unstable zone. The operational point with  $\beta_N = 2.56$ ,  $Q = 5$  for  $q_{min} = 2.4$  is stable and is close to the no wall limit  $\beta_N \approx$

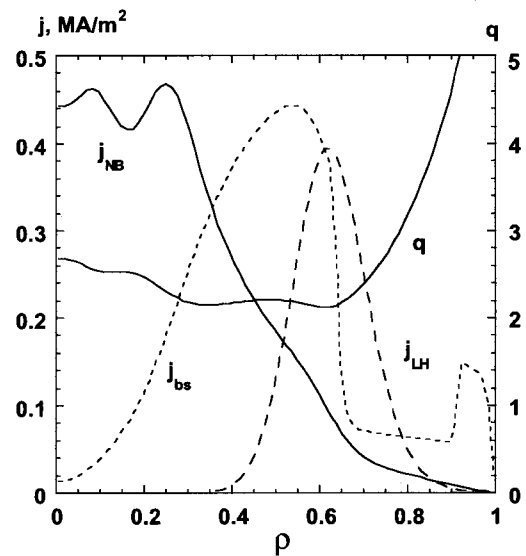


Fig. 5 Calculated profile of the safety factor  $q$  and densities of the bootstrap current ( $j_{bs}$ ), neutral beam driven current ( $j_{NB}$ ), and lower hybrid wave ( $j_{LH}$ ) driven current. The minimum  $q$  value is above 2.

Table 2 ITER plasma parameters for the SS scenario with different  $q$  profiles

	Unstable	Stable
$P_{LH}$ (MW)	29	33.7
$q_{min}$	2.1	2.4
$l_i$	0.72	0.63
$\beta_N$	2.8	2.56
$Q$	5.7	5
$\langle z_{eff} \rangle$	2.2	2.17
$P_{fus}$ (MW)	361	338

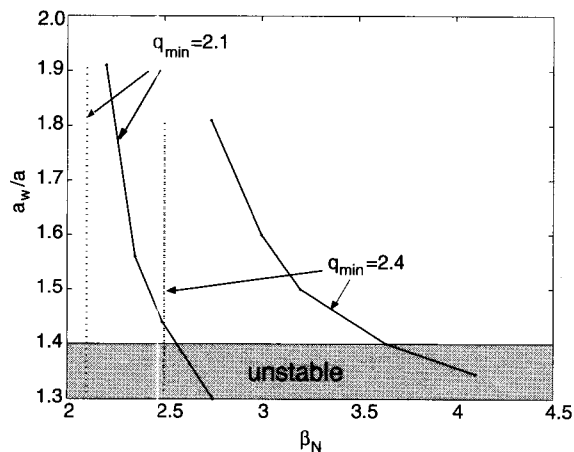


Fig. 6 Conducting wall position for stabilisation of the  $n = 1$  external kink mode  $a_w/a$  vs. normalised beta  $\beta_N$  for different  $q$  profiles and  $a = 1.85$  m. The no-wall limit is shown by dashed lines.

2.5 (see Fig. 6).

#### 4. Conclusions

The semi-empirical model used for ITER predictions satisfactorily reproduces experimental profiles from the profile database.

The semi-empirical approach predicts for ITER weak sensitivity of plasma performance to diffusivity profiles for similar boundary conditions.

The details of sawtooth modelling do not affect plasma performance provided the sizes of the mixing zone are similar and the ST period is longer than the pressure recovery time. The pressure gradient in the mixing zone is marginally stable vs. ballooning modes in the reference inductive scenario.

So, the reference ITER scenarios are robust against the considered effects.

High  $Q > 5$  steady-state operation would require stabilisation of low- $n$  ideal kink modes. There is an operational window with  $Q \geq 5$ ,  $\beta_N \geq 2.56$ , for the stabilising wall position compatible with the ITER design,  $a_w/a > 1.4$ .

This report was prepared as an account of work undertaken within the framework of ITER Coordinated Technical Activities (CTA). These are conducted by the Participants: Canada, the European Atomic Energy

Community, Japan, and the Russian Federation, under the auspices of the International Atomic Energy Agency. The views and opinions expressed herein do not necessarily reflect those of the Participants to the CTA, the IAEA or any agency thereof. Dissemination of the information in this paper is governed by the applicable terms of the former ITER EDA Agreement, which continue to apply during the CTA.

#### References

- [1] ITER Physics Basis, Nucl. Fusion **39**, 2175 (1999).
- [2] A.M. Dimits, A.M. *et al.*, Phys. Plasmas **7**, 969 (2000).
- [3] G.M. Staebler *et al.*, 18<sup>th</sup> IAEA Fusion Energy Conference, Sorrento, Italy (2000) TH4/1.
- [4] H. Nordman, P. Strand and J. Weiland, Nucl. Fusion **39**, 1157 (1999).
- [5] O. Kardaun *et al.*, 18<sup>th</sup> IAEA Fusion Energy Conference, Sorrento, Italy (2000) ITERP/04.
- [6] O. Kardaun, "On estimating the epistemic probability to realise  $Q = P_{\text{fus}}/P_{\text{ADD}}$  larger than a specified lower bound in ITER," Nucl. Fusion (2001), *in press*.
- [7] Y. Murakami *et al.*, J. Plasma Fusion Res. **77**, 712 (2001).
- [8] A.S. Kukushkin *et al.*, 18<sup>th</sup> IAEA Fusion Conference, Sorrento (2000) ITERP/10.
- [9] D. Boucher *et al.*, in Fusion Energy 1996 (*Proc. 16<sup>th</sup> Int. Conf. Montréal, 1996*) Vol. 2, IAEA, Vienna 945 (1997).
- [10] G.V. Pereverzev *et al.*, IPP 5/42 (1991).
- [11] D.E. Post *et al.*, Atomic Data and Nuclear Data Tables **20** (1977).
- [12] O. Sauter, C. Angoni and Y-R. Lin-Liu, Phys. Plasmas **6**, 2834 (1999).
- [13] P.H. Rebut *et al.*, Plasma Physics and Controlled Nuclear Fusion Research (*Proc. 12<sup>th</sup> Int. Conf. Nice, 1988*) Vol. 2, IAEA, Vienna 191 (1989).
- [14] ITER Physics Basis, Nucl. Fusion **39**, 2215 (1999).
- [15] A. Polevoi, H. Shirai and T. Takizuka, JAERI Data/Code 97-014 (1997).
- [16] ITER Physics Basis, Nucl. Fusion **39**, 2225 (1999).
- [17] F. Porcelli *et al.*, Plasma Phys. Control. Fusion **38**, 2163 (1996).
- [18] L. Degtyarev *et al.*, Comput. Phys. Comm. **10**, 103 (1997).